Three dimensional multi-pass repair weld simulations

22nd July 2004

Three Dimensional Multi-Pass Repair Weld Simulations

C D Elcoate[a], R J Dennis[a], P J Bouchard[b] and M C Smith[b]

[a]Frazer-Nash Consultancy Limited, 1 Trinity Street, College Green, Bristol, BS1 5TE, UK
[b]British Energy Generation Limited, Barnett Way, Barnwood, Gloucester, GL4 3RS, UK

Abstract

Full 3-dimensional simulation of multi-pass weld repairs is now feasible and practical given the development of improved analysis tools and significantly greater computer power. This paper presents residual stress results from 3-dimensional finite element analyses simulating a long (arc length of 62°) and a short (arc length of 20°) repair to a girth weld in a 19.6mm thick, 432mm outer diameter cylindrical test component. Sensitivity studies are used to illustrate the importance of weld bead inter-pass temperature assumptions and to show where model symmetry can be used to reduce the analysis size.

The predicted residual stress results are compared with measured axial, hoop and radial through-wall profiles in the heat affected zone of the test component repairs. A good overall agreement is achieved between neutron diffraction and deep hole drilling measurements and the prediction at the mid-length position of the short repair. These results demonstrate that a coarse 3-dimensional finite element model, using a "block-dumped" weld bead deposition approach (rather than progressively depositing weld metal), can accurately capture the important components of a short repair weld residual stress field. However, comparisons of measured with predicted residual stress at mid-length and stop-end positions in the long repair are less satisfactory implying some shortcomings in the finite element modelling approach that warrant further investigation.

Keywords: Weld modelling, Residual stress, Multi-pass, Finite element

1. Introduction

Structural integrity assessments for pressure vessels and piping are increasingly used to support the economic and safe management of operating power plant. Where welds are not stress-relieved, it is vital to have a good description of the residual stress field to perform an accurate assessment. Tensile residual stress generally has an adverse effect on component life. When combined with stresses due to service loads, tensile residual stress reduces crack initiation life, accelerates growth rates of pre-existing or service-induced defects, and increases the susceptibility of structures to catastrophic failure by fracture. Conversely, compressive residual stress can improve structural performance.

Reliable characterisation of residual stresses at non-stress-relieved welds is notoriously difficult. A commonly used approach for structural assessments is to assume bounding residual stress profiles, for example see R6 [1] or API 579 [2]. However, these profiles over-estimate the tensile residual stress levels, and for some classes of weld, there is a lack of consensus between different published compendia about the upper bound residual stress distribution [3]. Measurement of residual stress can be expensive and time consuming, hence there is a growing trend towards the use of advanced finite element (FE) systems for modelling the generation of residual stresses and material phenomena during welding, and a considerable amount of literature exists describing analyses that have been carried out. For example, see the bibliography of [4].

Full 3-dimensional (3-D) simulation of fusion welding processes, for the purpose of predicting residual stresses, is now feasible and practical given recent developments in computing capabilities. For example, Elcoate et al. [5] have recently simulated the residual stress field induced by the progressive deposition of a single manual metal arc (MMA) weld bead onto a stainless steel flat plate. The present paper describes the application of similar 3-D residual stress simulation techniques to analyse finite-length multi-pass weld repairs in a typical engineering component (a pipe). The accuracy of these predictions is then assessed via comparisons with residual stress measurements reported by Bouchard et al. [6].

Two weld repairs to a girth weld in a 19.6mm thick, 432mm outer diameter (OD) cylindrical test component are examined. The repairs have different lengths (arc lengths of approximately 20° and 62°), but are similar to each other in all other respects. The repairs are offset from the girth weld centre-line representing the practical case where there is a need to rectify lack of side-wall fusion defects, or degraded heat affected zone material. The repair cavities are relatively deep (70-75% of the wall thickness) and required 12 repair weld passes to completely fill. Extensive residual stress measurements have been carried out on the test component before and after repair using surface hole drilling, deep hole drilling and neutron diffraction techniques. Details of the

measurement techniques and results are not described here as they are fully documented elsewhere, see Bouchard et al. [6]. The FE studies presented in this paper were performed after completion of the residual stress measurements programme. A primary objective was to obtain a more accurate and more detailed prediction of the measured residual stress field than obtained using simplified models, see Dong et al. [7].

The residual stress simulations make use of a hybrid methodology coupling the FE codes FEAT [8] and ABAQUS [9] in series to carry out the thermal and mechanical parts of the analysis, respectively. This hybrid approach exploits the powerful thermal modelling capabilities offered by FEAT and the robust and efficient elastic/plastic solver in ABAQUS, and uses the flexibility provided by the FEAT command language to facilitate the 'coupling' between codes. Results from four separate FE weld simulation analyses are presented, investigating the sensitivity of the predicted residual stress field to repair weld length, assumed inter-pass temperature and mechanical boundary conditions (½ vs ¼ global symmetry). The most relevant results are compared with the residual stress measurements to assess the adequacy of the modelling approach employed.

2. Repair Weld Test Specimen

Two ex-service power station steam headers, 432mm outside diameter by 63.5mm thick, were used to fabricate the test component. The original header stainless steel material specification was ASME II: 1968 SA-182F-316H. The headers were bore-machined to an average thickness of 19.6mm and then solution heat treated (for 1 hour at 1050°C followed by air cooling) to remove any remnant residual stresses. One end of each header was further machined to form a J-groove girth weld preparation, and then the ends were butt welded together using a MMA procedure typical of that employed for steam raising pipe welds. No post-weld heat treatment of any kind was carried out.

Two weld repairs were subsequently made to the girth weld using typical manufacturing practice. A 'short' repair (arc length of ≈20°) was introduced centred circumferentially at 70° from top dead centre (TDC), and a 'long' repair (arc length of 62°) centred at 240° from TDC (Fig. 1). Here the arc lengths of the repairs are defined to be the effective length of the excavation at the ½-depth radius. The circumferential positions of the repairs were carefully chosen to minimise interaction effects with each other and with the header nozzles at TDC. The repair cavities were excavated using grinding tools and rotary burrs to a depth of 70 to 75% of the thickness of the wall (≈14-15mm). The cavities were offset from the centre-line of the original weld by about 12mm (see Fig. 1), representing a typical workshop situation where fabrication side-wall defects had been found in the original girth weld and required repair. The side-wall angles of both repairs were ~30° to the vertical, and the run-outs at the ends were at 45°. A tracing of a silicone replica impression from the short repair excavation is shown in Fig. 2. This impression is also representative of the long repair. Three passes laid with 2.5mm MMA electrodes and nine passes laid with 3.2mm electrodes were used to fill each repair cavity. The long repair was welded first and the short repair second. The mean measured heat inputs for the short and long welds of 1.47kJ/mm and 1.38kJ/mm were very similar to the estimated girth weld heat input of 1.4kJ/mm. Successive passes in each repair were deposited without time gaps, allowing the local inter-pass temperature to increase. Although the inter-pass temperatures were not recorded for these welds, local surface temperature measurements on a similar repair reached a steady state value of about 150°C after 4 repair passes. Special care was taken with the repairs to control the sequence of the capping passes. The pass sequence assumed for the filling passes and recorded for the capping passes for both welds is shown schematically in Fig. 2. The repair weld beads were deposited moving in the same circumferential direction. This resulted in all the long repair passes stopping at the 270° position. The final capping pass for each repair lies over the centre-line of the original girth weld.

Residual stresses after repair were measured in the repair weld HAZ along a line at -24mm (see Fig. 2b) at mid-length of the short repair, and both at mid-length and at the stop-end of the longer repair. The measurements were made using both the deep hole drilling technique and neutron diffraction, see Bouchard et al. [6] for details. Note that for the latter measurements, an access slot had to be machined near TDC for the neutron beam to pass through.

3. Repair Weld FE Simulation

3.1 General Considerations

A comprehensive review of FE modelling issues involved in the simulation of welding has been carried out recently by Lindgren [10, 11, 12]. More general guidance for modellers carrying out FE weld residual stress simulations suitable for 'fitness for service' integrity assessments (where very short wavelength stresses are ignored) can be found in WRC Bulletin 476 [13]. Although full 3-D simulation of fusion welding processes using a moving heat source is now feasible for the simple case of a single weld bead deposited on a flat plate [5], 3-D simulation of multi-pass welds in complex engineering components is more challenging. This is primarily because of demanding computer run-time and data storage requirements for large 3-D FE models. Consequently, an over-riding constraint in any 3-D multi-pass weld simulation study is the need to create a model that can be solved in a practical time-scale. To achieve this goal, compromises in the modelling approach have to be made based on engineering judgement in order to meet the analysis objectives.

The primary purpose of the present FE studies was to develop a sufficiently accurate simulation of the 3-D residual stress field in the HAZ adjacent to the short and long repairs in the test specimen, to achieve a reasonably good comparison with the measured through-wall residual stress profiles.

At the outset it was decided to ignore residual stresses from the initial girth weld and assume that the repair weld would locally dominate the final residual stress field of interest. Evidence supporting this assumption can be found in the 3-D shell FE weld simulation studies reported by Dong et al. [7]. However, it was judged important to represent the original weld material properties in the repair models.

Secondly it was assumed unlikely that stress variations along the weld repair arising from moving heat source and progressive weld metal deposition effects would have been resolved by the residual stress measurements. Here it is worth considering the expected distribution of residual stress along the welding direction of finite length repair welds, based on the moving heat source weld simulation results of Elcoate et al. [5] for a finite length weld bead-on-plate.

a) Bulk transverse contraction of the deposited weld metal is resisted by the global restraint of the structure, and this induces a long-range residual stress distribution which is self-equilibrating in the plane of the weld. This has a high magnitude tensile zone in the vicinity of the weld deposit, with a size-scale approximately equal to the length of the weld.

b) Temperature decay gradients in the wake of the moving weld torch induce a medium-range transverse residual stress distribution of relatively low magnitude. This has a tensile zone with a size-scale equal to about one half of the length of the bead.

c) Weld start and stop transient temperature effects induce very short-range residual stress perturbations having a size-scale of the order of the length of the weld pool.

The long-range effect (a) depends on the structural restraint of the component geometry (e.g. the length and thickness of plates or radius of curvature of shell structures), the repair geometry (length, depth and width) and the welding conditions. For single weld beads, medium-range effect (b) will depend on the welding advance rate, weld heat input and material properties. Short-range effect (c) will depend on the welding torch size. In multi-pass repair welds, effects (b) and (c), which enhance stresses in individual beads, are expected to be partially or fully relieved by thermal plasticity associated with successive passes. In addition, the start/stop positions of MMA beads in successive layers will rarely coincide. Thus, effects (b) and (c) are likely to be of concern only for the final capping passes.

The single bead on plate study [5], also compared the residual stresses generated by a 3D moving heat source simulation with those generated by a simplified 3D simulation in which the entire weld bead was deposited simultaneously (called "block-dumping"). Comparison of the two simulations showed that the block-dumping approach produces a good estimate of the long-range (type (a)) residual stresses. Thus it should be possible to obtain a good estimate of the long-range residual stress distribution in a multi-pass repair without resorting to a moving heat source simulation. This is an important simplification, and has major implications for the complexity of the finite element models and the duration of the analyses.

3.2 3-D FE Models

Three 3-D FE models of the welded test specimen were constructed as follows:

a) 'Short' repair – a one quarter 3-D FE model of a pipe with a short repair weld (arc length of approximately 20°). The model was constructed with 31972 nodes and 6939 elements.

b) 'Long' repair base-line – a one quarter 3-D FE model of a pipe with a long repair weld (arc length of approximately 62°). The model was constructed with 36180 nodes and 7922 elements.

c) 'Long' repair sensitivity – a one half 3-D FE model of a pipe with a long repair weld (arc length of approximately 62°). The model was constructed with 44265 nodes and 9742 elements.

In each case, symmetry was used to reduce the FE model size. A symmetry plane at the repair mid-length could be adopted because weld passes were block-dumped (see Section 3.3). Use of a further symmetry plane at 90° to the repair mid-length in the quarter models resulted in two repairs being deposited simultaneously on opposite sides of the pipe. The half model of the pipe with a long repair was used to assess the significance of the latter approximation.

In each model, the repair cavity was axially offset by 12mm from the original girth weld centre-line, and deposition of twelve repair weld passes simulated. A crude trapezoidal idealisation of each weld bead was adopted to minimise the model size and simplify its construction, see Figs. 3a and 3b. Thus each bead height was represented by a single element with the exception of the capping passes (10 to 12) which were two elements deep.

The meshes were constructed using ABAQUS 20-noded brick elements of type C3D20R (reduced integration) and C3D20RH (reduced integration, hybrid with linear pressure). Reduced integration, hybrid elements were assigned to a region of the model up to approximately 45mm either side of the repair weld. Hybrid elements were chosen for this region as large plastic strains (i.e. incompressible deformation) may occur during the welding process. When the material response is incompressible (or near incompressible, i.e. at large plastic strains) the solution to a problem cannot be determined in terms of the displacement history only, since a

purely hydrostatic pressure can be added without changing the displacements. Hybrid elements solve this problem by treating the pressure stress as an independently interpolated solution variable. Elsewhere in the model reduced integration elements were used.

A layer of weld boundary elements surrounding the repair weld approximately 2mm in thickness was included to represent melted parent material adjacent to the weld filler. These elements were assigned weld material properties. The predicted weld fusion boundaries were all contained within this boundary.

3.3 Thermal Analysis

The FE code FEAT [8] has been used successfully for 3-D thermal transient analyses of repair welds and coupled robustly with ABAQUS for 3-D residual stress analysis of a single weld bead-on-plate problem [5]. In this development work, it was shown that a simplified block-dumped modelling approach, where the entire length of a weld pass is deposited simultaneously, can give a good approximation of the residual stress field induced by a more realistic moving volumetric heat source analysis simulating progressive weld metal deposition. However, in applying the simplified approach it must be assumed that the welding torch start/stop transients and steady state wake temperature gradients associated with making a multi-pass repair can be ignored (see discussion in Section 3.1).

The present multi-pass repair weld analyses simulated the deposition of each repair pass using the block-dumped modelling approach in order to minimise the analysis size and computer run time. However, it was found that a stable thermal transient solution could not always be achieved when weld beads were introduced into the model using a time-dependent spatially varying heat-flux (i.e. a volumetric heat source), because the mesh was too coarse in regions of extreme temperature gradient local to the bead. The problem was overcome by employing an alternative 'fixed temperature' heat modelling approach. This involved introducing the weld filler metal into the FE model at an initial uniform temperature above the material melting point and holding it at this temperature until the transient energy input to the surrounding material was equal to the required weld heat input. After a given heating period the weld is allowed to cool via convection and also conduction as energy continues to flow into the substrate. This procedure was readily implemented by integrating the heat flux across the weld bead/substrate interface with respect to the area and time, using the HTFLUX functionality within FEAT. Weld pass 1 was introduced into the FE model at an uniform initial temperature of 1500°C and the remaining passes (2 – 12) at an uniform temperature of 1550ºC. These temperatures were chosen to give parent/weld substrate melted zone depths judged to be consistent with the weld pass heat inputs. The heat inputs for each idealised bead were derived from the test component measured data (weld pass heat inputs and cross-sectional areas of the excavations), to give a constant heat input per unit cross-section area of filler metal.

After deposition of each weld pass the model was allowed to cool down until the maximum temperature at any position along the deposited bead reached the specified inter-pass temperature for each pass: that is 130°C for pass 1, 150°C for pass 2 and 160°C for passes 3 to 11. After the final pass (pass 12) the model was allowed to cool to ambient conditions. To investigate the effect of a higher inter-pass temperature a sensitivity study was performed on the long repair base-line model where the temperature was set to 200°C for all passes (the upper limit in common welding procedures for stainless steel pipe welds).

All passes were individually modelled in the analysis but were initially de-activated from the solution, except for the first pass. When the thermal transient was complete for each pass the next weld bead was re-activated into the solution and the appropriate thermal transient initiated. This process was repeated until all passes had been introduced. The assumed bead deposition sequence is shown in Figure 3 with the last capping pass being made over the centre of the original girth weld.

Adiabatic boundary conditions were applied to the global symmetry planes. During the bead deposition (heat input) phase of any pass, convective and radiative heat transfer boundary conditions were applied to all external surfaces of the active elements in the model (including the pipe ends) with the exception of the current bead external surfaces and the symmetry planes. On completion of the bead deposition phase, convective and radiative heat transfer boundary conditions were also applied to the external surfaces of the current bead. Heat transfer coefficients of $2.1 W/m^2K$ and $7.6 W/m^2K$ were assumed for the internal and external surfaces of the pipe respectively and an emissivity of 0.35 was assumed for all surfaces. Measured temperature-dependent thermo-physical properties (thermal conductivity, specific heat, and density) for the parent and weld metal up to the material melting point of 1400ºC were used in the analysis, see Fig. 4. Above this temperature, properties were held constant, except for the thermal conductivity which was artificially increased to compensate for the effect of heat transfer due to convection stirring in the molten weld pool. The effects of latent heat of fusion were considered to be second order and therefore ignored to improve the thermal solution stability.

3.4 Mechanical Analysis

The repair weld simulation mechanical analyses were performed using ABAQUS 6.2 [9]. The only loads imposed on the model were transient nodal temperature data written by FEAT and included as a series of step definitions in the ABAQUS input deck for each weld pass. Each weld pass was added sequentially within ABAQUS using the *MODEL CHANGE option. The analyses were carried out using small displacement theory with isotropic material hardening

behaviour. Temperature-dependent thermal expansion, Young's modulus, Poisson's ratio and yield properties up to melting point were compiled for the mechanical analysis from both proprietary sources and from tensile tests on ex-service header and weld materials, see Figs. 4 and 5. A rate independent, isotropic elastic-plastic material model with strain hardening up to ~10% strain was used for the parent material. Weld metal was modelled as elastic-perfectly plastic with the yield strength equal to the 1% proof stress of weld material. Plastic strain annealing on melting was included in the analysis with a cut off temperature of 1400°C, following the studies of Elcoate et al. [5] showing the significance of annealing on stresses local to a weld bead.

4. Repair Weld Simulation Results

4.1 Thermal Analysis Results

The best measure of the adequacy of the FE thermal model for a weld pass is to compare predicted near-field and far-field transient temperatures with measurements. However, no such measured data were obtained for the welded test specimen. A more pragmatic and widely used measure is to compare the predicted fusion profile against observed macro-graphs of the weld [13], although this is not necessarily a sufficient condition to ensure that the weld 3-D conduction solution has been adequately represented in an FE model.

The plots shown in Fig. 6 illustrate the predicted maximum extent of the melting temperature (1400°C) isotherm calculated from the peak temperatures at all nodes at any time during the transient for passes 1 and 2 of the short repair. These short repair results are representative of those from long repair models including the high inter-pass temperature sensitivity study.

The predicted areas of melted parent/weld substrate and fusion zone shapes were judged to be consistent with expected fusion boundaries for the weld pass heat inputs, despite the somewhat crude layered trapezoidal weld bead idealisation in the FE model. A more quantitative assessment of the weld simulation heat input model will be performed once the test component has been destructively examined and a cross-section of the weld etched to reveal the fusion zone patterns.

The maximum inter-pass temperature always occurred at mid-length of the bead owing to the model symmetry, and was controlled not to exceed 160°C in the base-line models. As successive repair passes were laid down, the volume of the pipe at elevated temperature steadily increased.

4.2 Mechanical Analysis Results

The weld mechanical analyses produced a complete picture of the residual stress field induced by long and short weld repairs. A small subset of the predicted results from both repairs is presented here on a radial-circumferential plane beneath the first capping pass of the repair weld (see Figs. 2 and 3). Detailed residual stress results from the long repair sensitivity analyses allow an assessment to be made of the weld modelling symmetry conditions and inter-pass temperature assumptions. In addition, predicted results from the short and long repairs are compared with each other to illustrate the effect of repair length. Comparisons of predictions for each repair length with corresponding residual stress measurements are discussed later in Section 5.

Consider first the long repair. Figures 7a and 7b show the through-thickness variation of hoop and axial stresses (see Fig. 1a for notation) for a number of circumferential locations along the long repair weld. Results are presented starting at the model symmetry plane at mid-length of the repair, (0°) and then at 10°, 20°, 30°, 31.4°, 40°, 50° and 60°. The repair excavation is at full depth up to 31.4°, at which point the 45° run-out commences.

The axial stress (Fig. 7b) is highest at the inside surface, with a subsidiary peak just below the outer surface adjacent to the repair weld cap. The shape of the stress profile is similar at the various circumferential positions along the length of the repair weld, although the peak near the outer surface increases in magnitude towards the repair end. Beyond the repair end between 40° and 50° the axial stresses are highly compressive. They then reduce in magnitude with increasing circumferential distance from the repair. The shape of the hoop stress profile (Fig. 7a) is similar along the length of the repair weld (0° to 31.4°), changing beyond the repair end to a linear bending profile of opposite gradient to within the repair. It should be noted here that the original girth weld residual stress field, which was not modelled, would significantly influence the residual stress field beyond the ends of the repair.

A powerful way to understand a residual stress field and the structural behaviour of a welded joint is to decompose the residual stress distribution along a line into a 'membrane' component, a 'through-wall bending' component and a self-equilibrated component of stress. The membrane component is defined as the uniformly distributed stress giving the same integrated force and the bending component is the linearly varying stress along the line, after subtraction of any uniform stresses (membrane), giving the same moment result. For example, decomposing the through-wall stress profiles from the ¼-model base-line case shown in Fig. 7 produces the variation in linearised stresses around the circumference shown in Fig. 8. From Fig. 8b it is evident that the repair weld has introduced a significant tensile axial membrane stress along the entire length of the repair and that this tensile zone is self-equilibrated by highly compressive stresses beyond the repair end. The compressive zone is distributed over a circumferential arc-length approximately equal to one half the length of the tensile zone (≈35°). The repair has also induced a significant axial through-wall bending stress that is tensile at the inner surface. The sign of the bending stress implies that radial contraction of the repair has introduced a 'tourniquet' loading that dominates local bead to bead

contraction. This type of behaviour is similar to that observed for high heat input pipe girth welds [3].

Figure 8 also compares the long repair base-line ¼-model results with the ½-model and 200°C inter-pass sensitivity analyses. Overall the distributions of linearised hoop and axial stresses from the three models are very similar to each other, but there are important differences in detail. At the repair mid-length the magnitude of the axial membrane stress for the 200°C inter-pass temperature case is about 20% greater than for the other two models with 160°C maximum inter-pass temperatures. The inter-pass temperature also has a significant effect on the axial bending component of stress along the repair, and on the hoop membrane and bending stress magnitudes in the same region. Beyond the ends of the repair inter-pass temperature has little effect on any stress component.

The model symmetry conditions have little effect on the stresses within the repair length, apart from the hoop bending stress (Fig. 8a). However, beyond the immediate influence of the repair (i.e. > ½ repair length beyond end), it is evident that the use of a ¼-model for this length of repair is introducing significant errors in the stress distributions (Figs. 8a and 8b).

Figures 9a and 9b compare the through-wall distributions of hoop and axial stress at the repair mid-length from the three long repair models (note that Fig. 9 also includes measured stresses that are discussed later). These detailed profiles confirm the importance of the inter-pass temperature on the resultant stress distribution and local magnitude of residual stress at the inner surface.

Now consider the short repair. Figures 10a and 10b show through-wall hoop and axial stress distributions for the short repair. Results are presented starting at the model symmetry plane at mid-length of the repair (0°), and then at 5°, 11.2°, 14.8°, 20°, 30°, 40° and 60°. The repair excavation is at full depth up to 14.8°, at which point the 45° run-out commences. Hoop and axial stress profiles within the short repair are similar in through-wall distribution to the long repair (see Fig. 7), but much greater in magnitude. Figures 11a and 11b compare the variation in linearised stresses around the circumference for the short repair with the long repair base-line model. The most notable difference between the repairs is that the magnitude of axial membrane stress in the short repair is substantially larger than for the long repair.

5. Predicted vs Measured Residual Stresses

5.1 Short repair

Figures 12 and 13 compare measured and predicted through-thickness stress profiles in the pipe axial, radial and hoop directions at mid-length of the short repair. Overall, the correlation between measurements and predictions is good. The magnitudes of the decomposed axial membrane and bending stresses are almost identical, see Table 1, although there are evidently differences in the self-equilibrated component of stress (see Fig. 14). These differences in the detailed profile may be associated with the weld pass sequence (which is unknown below the capping passes), the weld bead trapezoidal idealization, and the simple isotropic material hardening model employed. The predicted radial stresses (Fig. 12b) are very low, and confirmed by the neutron diffraction residual stress measurements. The measured and predicted hoop stress profiles also closely agree with each other (Fig. 13a). But this may be fortuitous as the magnitude of hoop stresses at a repair vary rapidly in the axial direction (see Fig. 13b), and therefore the measured profile will be sensitive to the pass deposition sequence and the exact location of the measurement line relative to the actual repair geometry.

The good general agreement between the measurements and prediction show that a fairly coarse mesh 3-D FE model, using a "block-dumping" approach, can accurately capture the important components of the residual stress field associated with a short weld repair. However, accurate prediction of the self-equilibrated component of stress needs a more detailed repair weld modelling approach than that adopted here. The repair self-equilibrated component of axial stress is likely to be the least significant in structural integrity fracture assessments, except for small length-scale cracks [14]. For example, consider through-wall growth of a semi-elliptic shaped outer surface-breaking crack by creep in the HAZ of the short repair weld (i.e. the -24mm position in Fig. 2a). Figure 15 shows the contributions of different components of residual stress to the stress intensity factor, K, for the measured and predicted stress profiles (Fig. 14). It is seen that the through-thickness self-equilibrated component of stress contribution to the total K becomes less important as the crack fractional depth increases, that is as the crack size increases relative to the residual stress length scale.

5.2 Long Repair

Comparisons between measured and predicted through-wall stress profiles for the long repair are shown in Fig. 16 for the repair stop-end position, and Fig. 9 for the mid-length position. The axial stress profiles have also been decomposed into membrane and bending components (see Table 1) to aid quantitative assessment.

At the stop-end position of the repair, the predicted and measured axial stresses correlate closely with each other over the inner half of the wall thickness, but diverge in the outer half (Fig. 16b). This divergence creates the significant difference between predicted and measured membrane and bending components of stress (Table 1). However, there are insufficient neutron diffraction measurements towards the outer surface of the pipe to capture the influence of the repair weld capping passes that clearly dominate the predicted residual stress field. The shapes of the predicted and measured hoop stress profiles are similar but the latter are

substantially more tensile than predicted. As noted above for the short repair in Section 5.1 (see Fig. 13b), the magnitude of the hoop stresses at a repair varies rapidly in the axial direction. Both the predicted and measured radial stresses (Fig. 16c) have very low magnitudes.

At mid-length of the long repair, the predicted and measured stresses show some significant differences. The measured membrane component of axial stress is much greater than predicted, although the correlation between bending components of stress is good (see Table 1). Given the close correlation between the deep hole and neutron diffraction measurements for the short repair (Figs. 12 and 13), it is reasonable to assume that the deep hole measurement technique is reliable for this type of weldment. Thus the results imply some significant shortcomings in the FE modelling approach. This could be associated with the influence of "block-dumping" the entire length of bead rather than progressively depositing weld metal or the isotropic material hardening behaviour assumed, or a combination of the two effects. A recent sensitivity study (not reported here) has shown that the discrepancy is not a large displacement effect. At the repair stop-end the shapes of the predicted and measured hoop stress profiles are similar but the latter are substantially more tensile than predicted. Further detailed residual stress measurements are planned on the test component as well as advanced FE studies to investigate and resolve the reasons for the poor correlations.

Residual stresses associated with the original girth weld were not represented in any of the repair weld FE analyses, although these would have been present in the test component. Repair weld simulation studies for other repair configurations (not reported here) were carried out by the authors that included the influence of an original repair residual stress field, but it was found that predicted stresses close to the repair were relatively unaffected by the prior stress field.

6. Conclusions

Residual stresses at a long (arc length of 62°) and a short (arc length of 20°) repair to a girth weld in a 19.6mm thick, 432mm OD cylindrical test component have been simulated using a 3-D FE procedure. The residual stress simulations coupled the FE codes FEAT [8] and ABAQUS [9] in series to carry out the thermal and mechanical parts of the analysis respectively. Various simplifications were implemented to reduce the model size including the use of a 'block-dumped' approach (i.e. the entire length of each weld bead was deposited simultaneously), and global symmetry resulting in two repairs being deposited simultaneously on opposite sides of the pipe.

All the FE simulations predicted that a finite length weld repair introduces an axial membrane stress of significant tensile magnitude along the entire length of the repair, and that this tensile zone is self-equilibrated by highly compressive stresses beyond the repair ends. The circumferential length scale of the compressive zone beyond each end of the repair was approximately equal to one half the length of the repair tensile zone. The repairs also induced significant axial through-wall bending stresses that were tensile at the inner surface, indicating a strong 'tourniquet' type of loading.

Increasing the modelled inter-pass temperature from 160°C to 200°C significantly increased (by ≈20%) the magnitude of the axial membrane stress as well as influencing both the axial bending component and hoop stresses within the repair length. Beyond the ends of the repair inter-pass temperature had little effect.

The model symmetry conditions had little effect on the stresses within the repair length. However, for the long repair (arc length of 62°) it was found that use of a ¼-model introduced significant errors in the stresses beyond the immediate influence of the repair (i.e. > ½ repair length beyond the end). Therefore care should be taken using such ¼-pipe symmetry conditions for repairs longer than about 60° arc-length.

The good overall agreement between measurements and prediction for the short repair demonstrates that a fairly coarse mesh 3-D FE model, using a "block-dumping" approach, can accurately capture the important components of the residual stress field. However, accurate prediction of the self-equilibrated component of stress at the repair needs a more detailed repair weld modelling approach.

Comparisons of measured and predicted residual stress at mid-length and the stop-end of the long repair were less satisfactory, implying some shortcomings in the FE modelling approach. This could be associated with the influence of "block-dumping" the entire length of the bead rather than progressively depositing weld metal or with the material hardening behaviour assumed, or with a combination of the two effects. Further detailed residual stress measurements and advanced FE studies are planned on the test component to investigate and resolve the reasons for the poor correlations.

7. Acknowledgments

The work was carried out within the European 5th Framework research project ENPOWER, co-funded by British Energy Generation Limited and the EC Nuclear Fission Safety Programme. This paper is published with permission of British Energy Generation Limited.

8. References

[1] Procedure R6 Revision 4: Assessment of the Integrity of Structures Containing Defects. Gloucester: British Energy Generation Ltd, Amendment 2, 2003.

[2] API Recommended Practice 579, First Edition. Washington, American Petroleum Institute, 2000.
[3] Bouchard P. J., Validated Residual Stress Profiles for Fracture Assessments of Stainless Steel Pipe Girth Welds, accepted for publication in Int. J. Pres. Ves. & Piping, 2004.
[4] Mackerle J., 2001, Finite element analysis and simulation of welding – an addendum: a bibliography (1996-2001), Modelling Simul. Mater Sci Engng 10:295-318.
[5] Elcoate C.D., Bouchard P.J. and Smith M.C, 2003, 3-Dimensional Repair Weld Simulations – Bead-on-plate Comparisons, ABAQUS World Users' Conference, Munich.
[6] Bouchard P.J., George D., Santisteban J.R., Bruno G., Dutta M., Edwards L.E., Kingston E., and Smith D.J., Measurement of the residual stresses in a stainless steel pipe girth weld containing long and short repairs, Int. J Pres. Ves. & Piping, Special Issue on Residual Stresses at Repair Welds, 2004, p.##-##.
[7] Dong, P., Zhang, J., Bouchard, P.J., Effects of Repair Weld Length on Residual Stress Distribution, Trans. ASME J. Pres. Ves. Techn., Vol. 124, No. 1, 2002, pp. 74-80.
[8] FEAT, Version 3.4.0, "Finite Element Analysis Toolbox User Guide", Serco Assurance, 2002.
[9] ABAQUS/Standard User's Manual, Hibbitt, Karlsson and Sorensen, Inc., Version 6.2, 2001.
[10] Lindgren L.E., 2001, Finite Element Modeling and Simulation of Welding Part 1: Increased Complexity, Jnl Thermal Stresses, 24:141-192.
[11] Lindgren L.E., 2001, Finite Element Modeling and Simulation of Welding Part 2: Improved Material Modeling, J Thermal Stresses, 24:195-231.
[12] Lindgren L.E., 2001, Finite Element Modeling and Simulation of Welding Part 3: Efficiency and Integration, Jnl Thermal Stresses, 24:305-334.
[13] Dong P. and Hong J.K., 2002, Recommendations for determining residual stresses in fitness-for-service assessment, WRC Bulletin 476, Welding Research Council, New York.
[14] Bouchard P. J. and Withers P. J., The Appropriateness of Residual Stress Length Scales in Structural Integrity, presented at Mecasens II, Sept 2003, accepted for publication in Journal of Neutron Research.

Table 1
Predicted vs measured membrane and through-wall bending components of axial stress in the HAZ at mid-length of the short repair.

A negative bending equates to tensile stress at the inner bore.
ND = Neutron Diffraction; DH = Deep Hole

Repair	Position	Membrane stress (MPa)	Bending stress (MPa)
Short	Measured at mid-length	185 (ND) 194 (DH)	-84 (ND) -98 (DH)
	Predicted at mid-length	176	-102
Long	Measured at mid-length	143 (DH)	-145 (DH)
	Predicted at mid-length	47	-114
	Measured at repair-end	36 (ND)	-141 (ND)
	Predicted at repair-end	116	-42

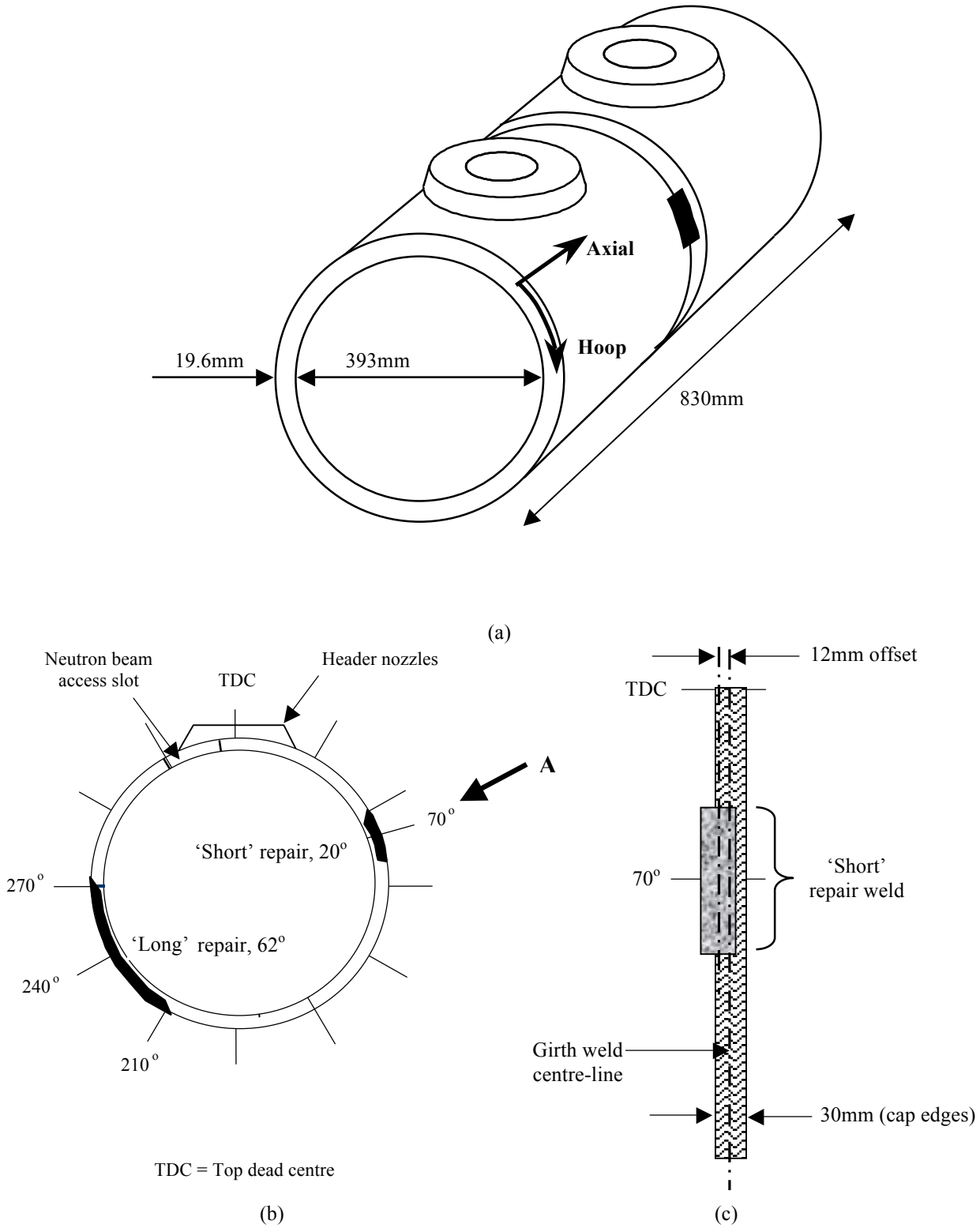

Fig. 1. a) General arrangement of mock-up component, b) Cross-section through girth weld showing circumferential positions of short and long weld repairs, and c) View on A of short repair showing offset.

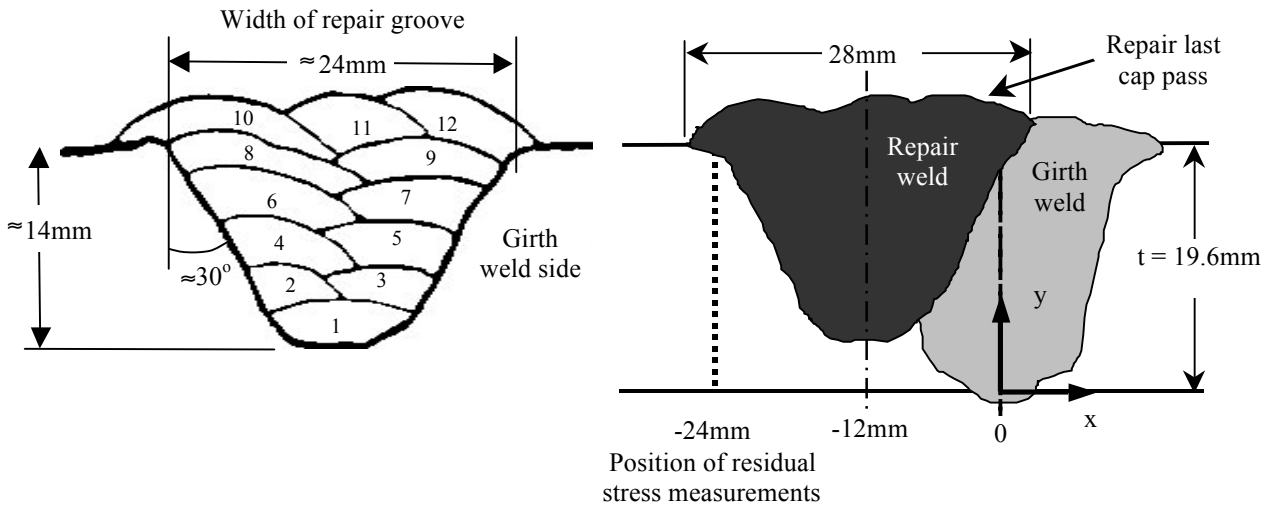

(a) (b)

Fig. 2. a) Short repair measured excavation profile with schematic bead lay-up, and b) Position of neutron diffraction and deep hole residual stress measurements (x = -24mm).

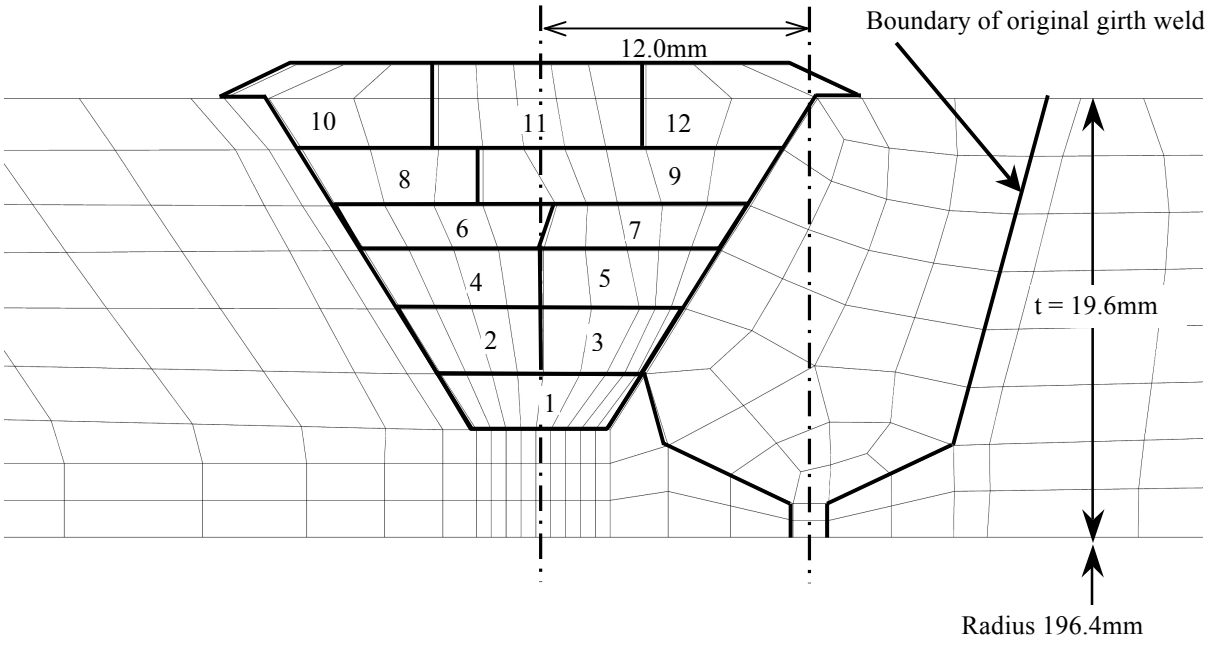

(a)

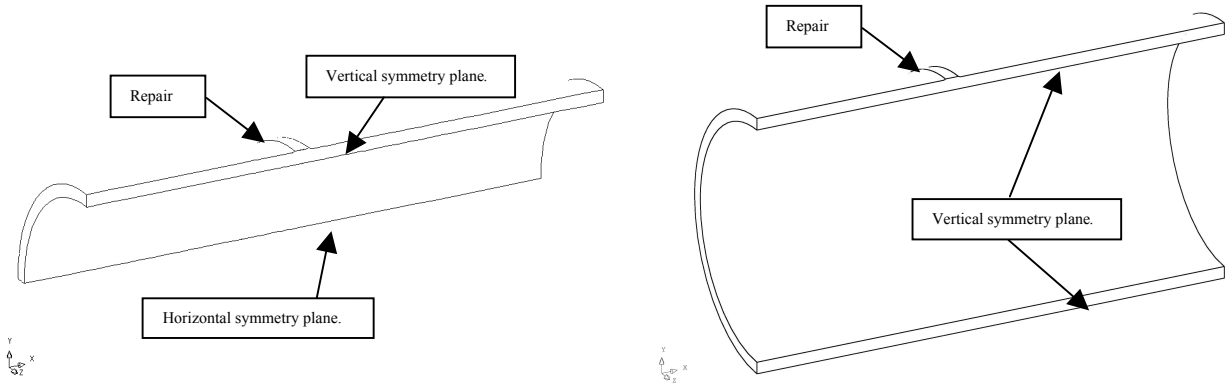

(b)

Fig. 3. Typical 3-D finite element model: a) Cross-section at mid-length of repair, and b) Full finite element model showing symmetry planes for quarter and half models.

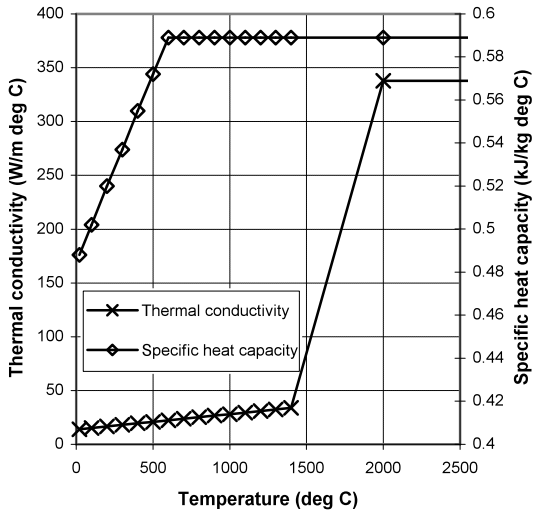

(a)

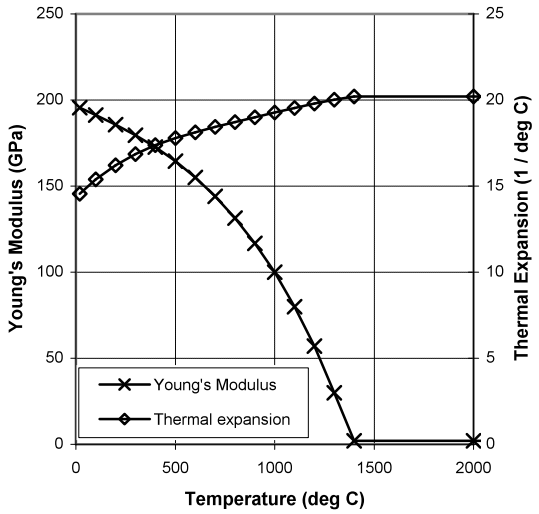

(b)

Fig. 4. Thermal Conductivity and Specific Heat Capacity variation with temperature (a) and Young's Modulus and Thermal Expansion variation with temperature (b).

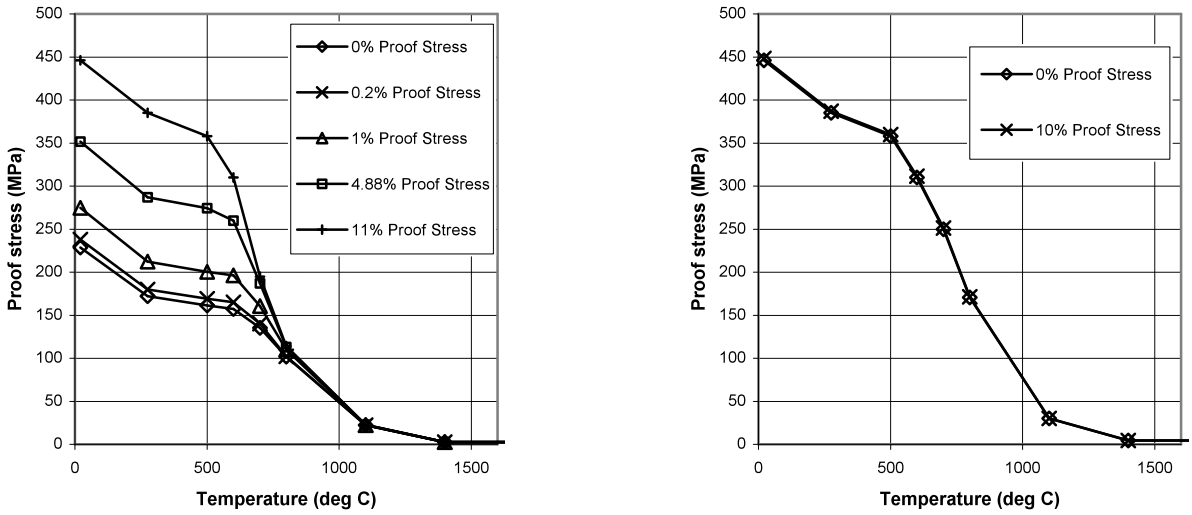

(a) (b)

Fig. 5. Variation of plastic properties (true stress and strain) with temperature: a) Parent material, and b) Weld material.

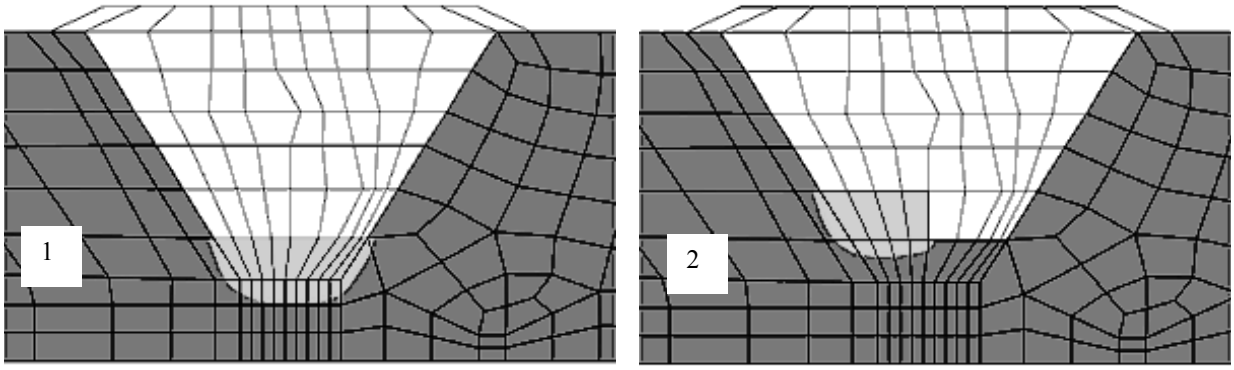

(a) (b)

Fig. 6. Predicted fusion zone (defined by maximum extent of 1400°C isotherm) at repair weld mid-length is indicated by the light shaded area for, a) Weld pass 1 and b) Weld pass 2.

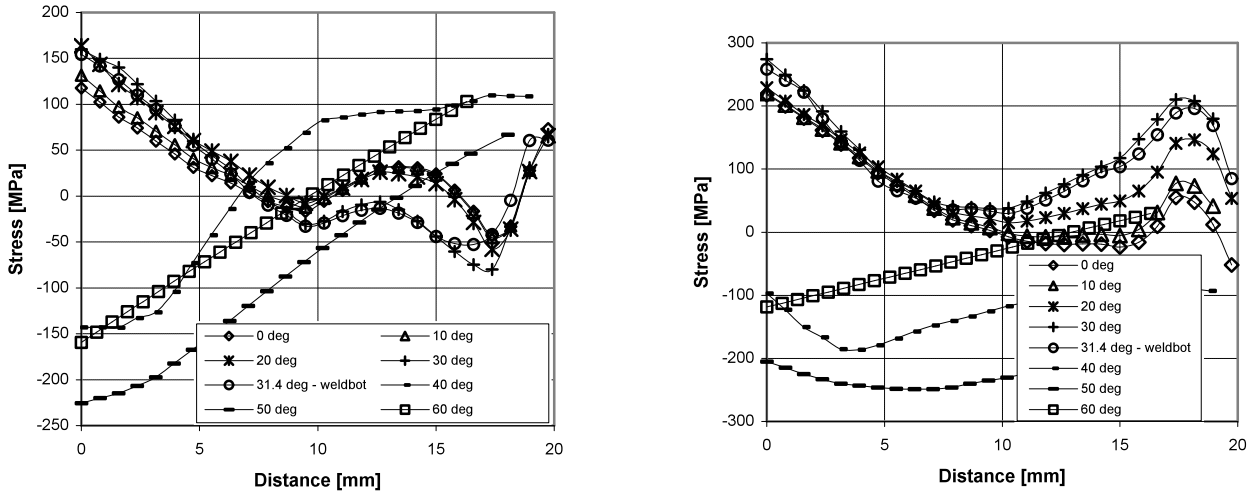

(a) (b)

Fig. 7. Predicted residual stress plotted through the wall thickness (from the inside surface) in the repair weld HAZ beneath the first weld cap pass at various angles from mid-length for the base-line long repair model: a) Hoop stress, and b) Axial stress.

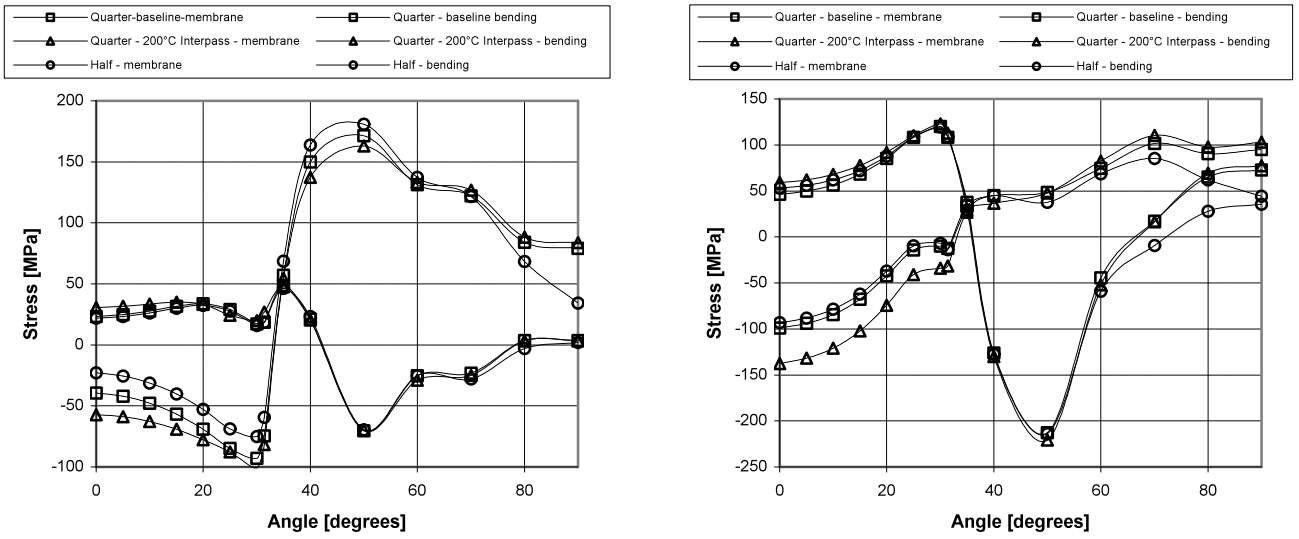

(a) (b)

Fig. 8. Linearised stresses (long repair weld HAZ beneath the first weld cap pass) plotted as a function of circumferential position for the base-line and sensitivity analyses (0° is at the repair mid-length, negative bending equates to tensile stress at the inner bore), a) Hoop stresses, and b) Axial stresses.

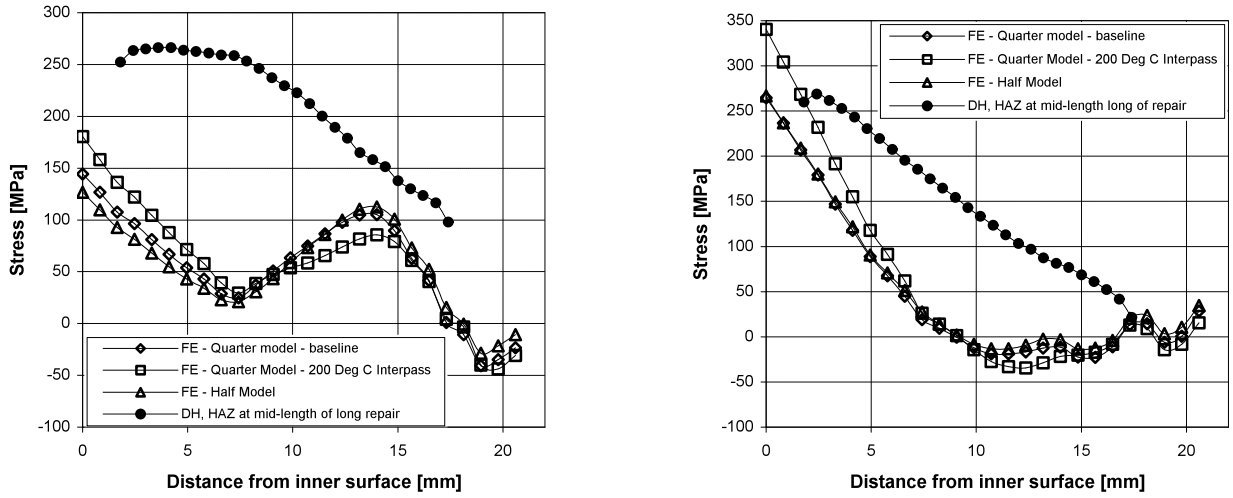

(a) (b)

Fig. 9. Comparison of the through-wall distributions of hoop (a) and axial (b) stress at the repair mid-length from the three long repair models and a deep hole (DH) measurement.

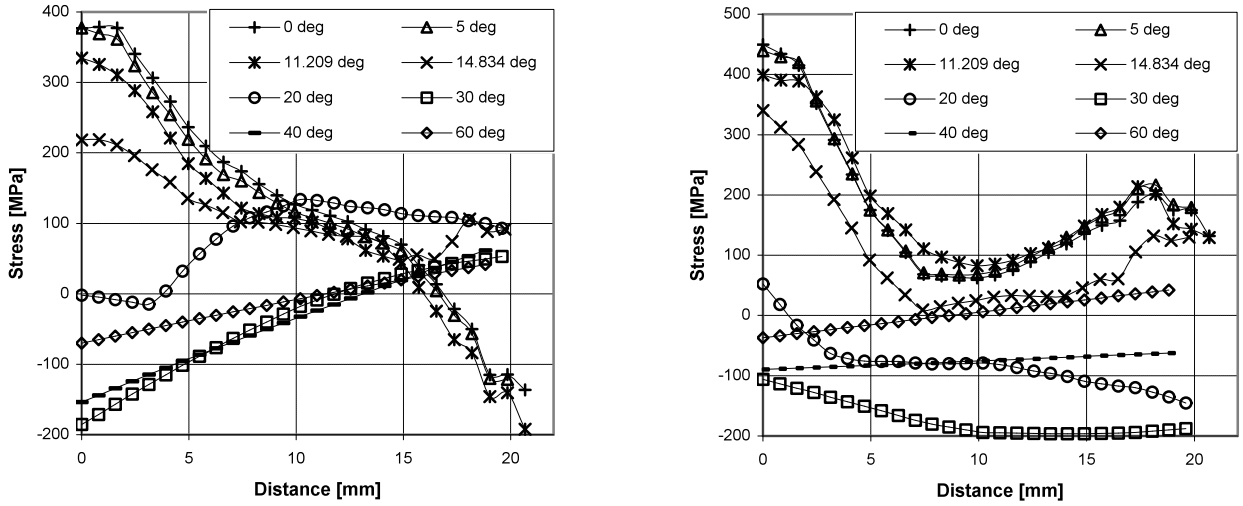

(a) (b)

Fig. 10. Hoop stress (a) and axial stress (b) for the short repair plotted along radial lines through the wall thickness in the repair weld HAZ, beneath the weld first capping pass.

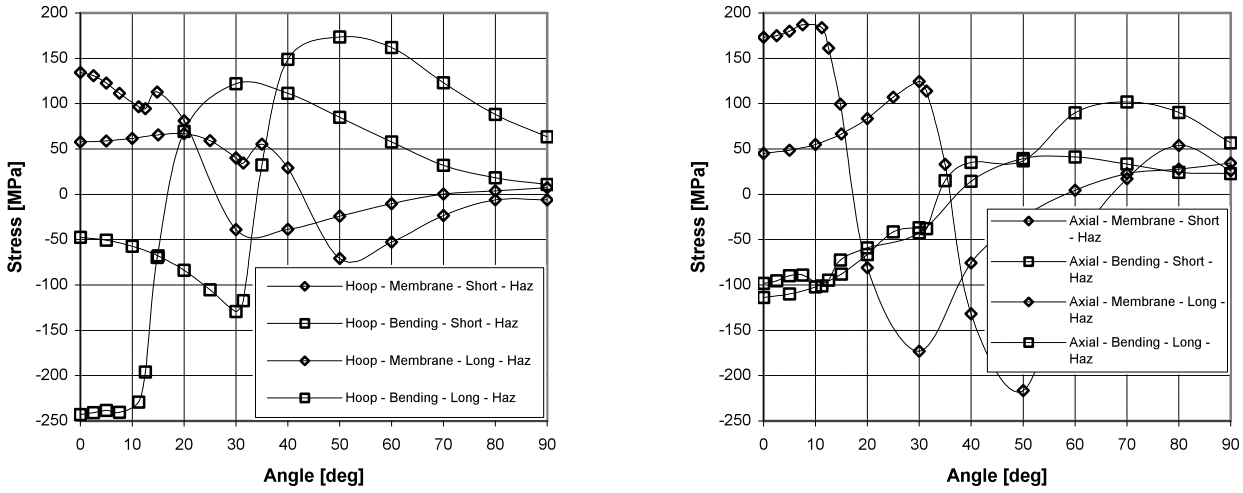

(a) (b)

Fig. 11. Variation in linearised hoop (a) and axial (b) stresses around the circumference for the short repair with the long repair base-line model.

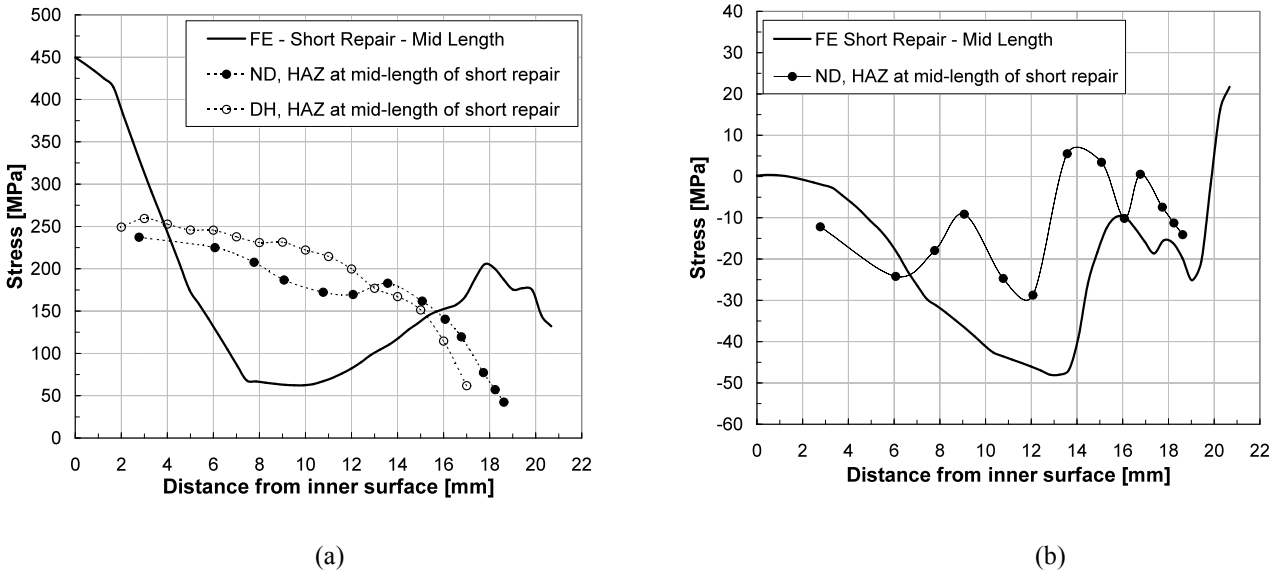

(a) (b)

Fig. 12. Comparison of measured and predicted stresses at mid-length of a short repair along a radial line in the repair weld HAZ beneath the first weld cap pass (x = -24mm): a) Axial stress, and b) Radial stress.

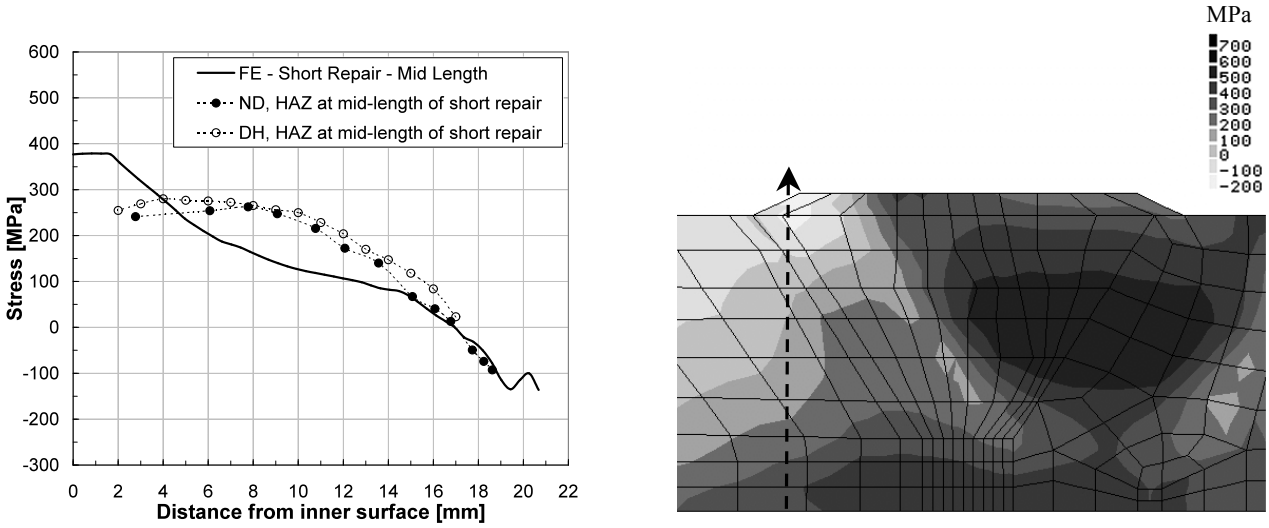

(a) (b)

Fig. 13. Comparison of measured and predicted hoop residual stresses at mid-length of a short repair along a radial line in the repair weld HAZ beneath the first weld cap pass (x = -24mm): a) Line plot and measurement comparison, and b) Contour plot of predicted stresses.

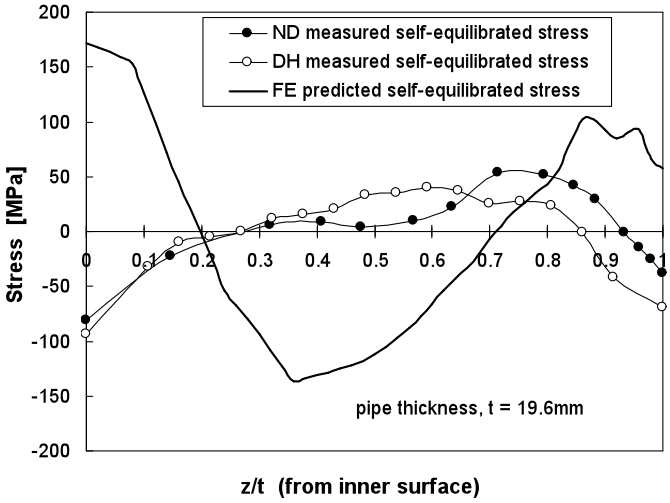

Fig. 14. Comparison of measured and predicted self-equilibrated components of axial residual stress at mid-length of the short repair (x = -24mm), see Fig. 12a.

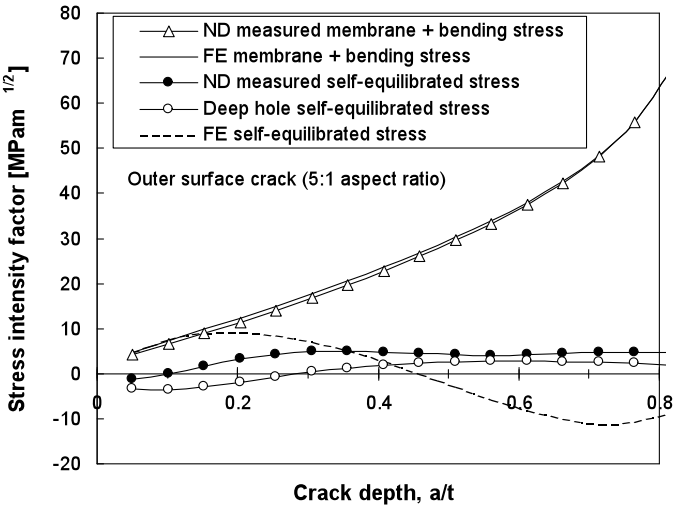

Fig. 15. Stress intensity factors for a circumferential surface crack (depth:surface length = 5:1) initiated on the outer surface at mid-length of the short repair at x = -24mm arising from different components of measured and predicted residual stress.

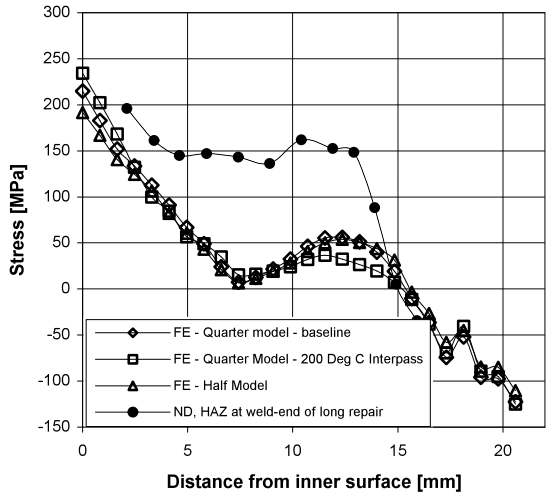

(a)

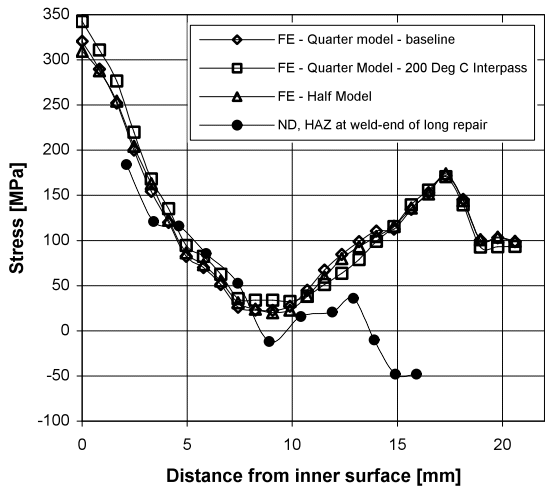

(b)

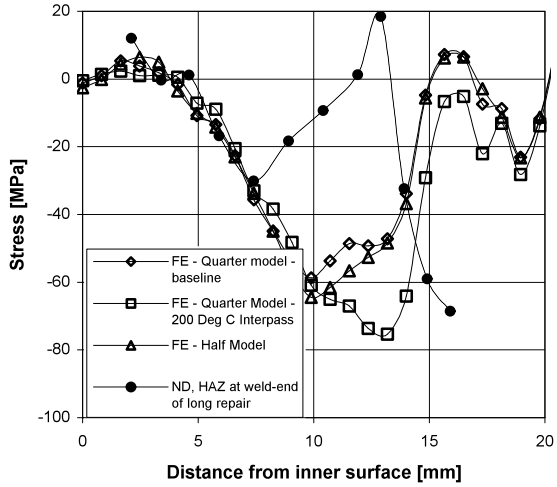

(c)

Fig. 16. Comparison of long repair measured v predicted results at weld end: a) Hoop stress, b) Axial stress, and c) Radial stress.